Pergamon

Int. J. Solids Structures Vol. 34, Nos 31–32, pp. 4127–4146, 1997

0020-7683/97 $17.00 + .00

PII: S0020-7683(97)00017-6

A SPHERICAL CAVITY-EXPANSION PENETRATION MODEL FOR CONCRETE TARGETS

M. J. FORRESTAL
Sandia National Laboratories, Albuquerque, New Mexico 87185-0303, U.S.A.

and

D. Y. TZOU
Department of Mechanical and Aerospace Engineering, University of Missouri, Columbia, Missouri 65211, U.S.A.

(*Received* 1 *March* 1996; *in revised form* 5 *December* 1996)

Abstract—We developed a spherical, cavity-expansion penetration model for concrete targets. Target constitutive descriptions idealized pressure–volumetric strain as incompressible or linear compressible and idealized shear strength–pressure as Mohr–Coulomb with a tension cutoff. We showed these idealized material descriptions were reasonable approximations to triaxial material data. Predictions from the compressible penetration model are in good agreement with depth of penetration data for a 30.5-mm-diameter, 1.60 kg, ogive-nose, rod projectile for striking velocities to 1100 m/s. © 1997 Elsevier Science Ltd.

INTRODUCTION

Analytical methods for penetration mechanics began with the work of Bishop *et al.* (1945). They developed equations for the quasi-static expansions of cylindrical and spherical cavities and used these equations to estimate forces on conical nose punches pushed slowly into metal targets. Later, Goodier (1965) developed a model to predict the penetration depth of rigid spheres launched into metal targets. That penetration model included target inertial effects, so Goodier (1965) approximated the target response by results from the dynamic, spherically symmetric, cavity-expansion equations for an incompressible target material derived by Hill (1948) and discussed by Hill (1950) and Hopkins (1960). Recently, Forrestal *et al.* (1995) developed spherical cavity-expansion penetration models for spherical-nose, rigid rods that penetrate ductile metal targets. Model predictions are in reasonably good agreement with depth of penetration data.

Cavity-expansion penetration models have also been used to study polycarbonate targets. Wright *et al.* (1992) present modeling and punch data, and Fleck *et al.* (1990) present material data that show high ductility at high strain rates is the main reason for the good ballistic performance of polycarbonate targets. Radin and Goldsmith (1988) and Wright *et al.* (1993) present these ballistic impact data.

Forrestal and Luk (1992) developed a spherical cavity-expansion model for soil targets and compared model predictions with field tests. Predictions were in reasonably good agreement with projectile deceleration and depth of penetration data. In addition Forrestal (1986) developed a cylindrical cavity-expansion model for penetration into dry, porous rock and compared predictions with projectile deceleration data. We observed that the cylindrical cavity-expansion approximation overpredicts the early time deceleration response and underpredicts the later deceleration response. By contrast, the spherical cavity-expansion approximation is in reasonably good agreement for the entire deceleration response (Forrestal and Luk, 1992).

In this study, we present a spherical cavity-expansion penetration model for concrete targets and compared predictions with depth of penetration data for a 30.5-mm-diameter, 1.60 kg, ogive-nose steel rod (Forrestal *et al.*, 1996). Spherical cavity-expansion penetration models approximate the two-dimensional target response with equations derived from

spherically symmetric, cavity-expansion analyses (Forrestal *et al.*, 1995). Thus, the spherically symmetric, cavity-expansion analyses are used as input to the penetration equations. Target constitutive descriptions idealize pressure–volumetric strain as incompressible or linear compressible and idealize shear strength–pressure as Mohr–Coulomb with a tension cutoff. We show later that these idealized material descriptions are reasonable approximations to triaxial material data (Joy and Ehrgott, 1993). In the following sections, we derive equations for the spherically symmetric cavity-expansion problems, present our penetration equations, and compare model predictions with depth of penetration data.

SPHERICALLY SYMMETRIC CAVITY-EXPANSION PROBLEM FORMULATION

A spherically symmetric cavity is expanded from zero initial radius at constant velocity V. As shown in Figs 1a, b, this expansion produces plastic and elastic response regions. For slow enough V, there are three regions of response (Fig. 1b): an elastic region, a region with radial cracks (the material reaches its tensile strength), and a plastic region (the material reaches its shear strength). As V increases, the radially cracked region diminishes and is eliminated eventually. That is, for large enough cavity-expansion velocity V, the response is elastic–plastic (Fig. 1a). In Fig. 1b, the plastic region is bounded by $r = Vt$ and $r = ct$, the cracked region is bounded by $r = ct$ and $r = c_1 t$, and the elastic region is bounded by $r = c_1 t$ and $r = c_d t$ where r is the radial Eulerian coordinate, t is times, c and c_1 are interface velocities, and c_d is the elastic, dilatation velocity.

The material in the plastic region (Forrestal and Longcope, 1990) is described by a linear pressure–volumetric strain relation and a Mohr–Coulomb yield criterion. Thus,

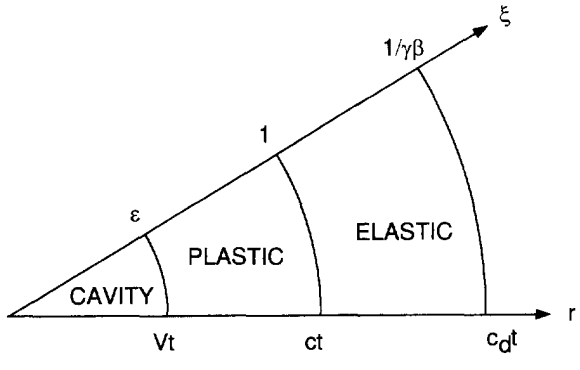

(a)

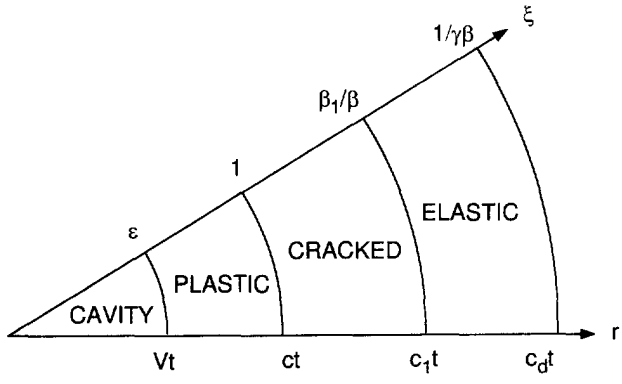

(b)

Fig. 1. Response regions: (a) the elastic–plastic problem and (b) the elastic–cracked-plastic problem.

$$p = K(1-\rho_0/\rho) = K\eta \tag{1a}$$

$$p = (\sigma_r+\sigma_\theta+\sigma_\phi)/3; \quad \sigma_\theta = \sigma_\phi \tag{1b}$$

$$\sigma_r-\sigma_\theta = \lambda p+\tau; \quad \tau = [(3-\lambda)/3]Y \tag{1c}$$

where p is the pressure; ρ_0, ρ are densities of the undeformed and deformed material, respectively; η is the volumetric strain; K is the bulk modulus; σ_r and σ_θ are radial and circumferential Cauchy stress components (positive in compression); λ and τ define the pressure-dependent shear strength; and Y is the uniaxial compressive strength.

The elastic region has material properties given by Young's modulus E and Poisson's ratio v, where E, is related to K by $E = 3K(1-2v)$. For the elastic region, the circumferential tensile stresses are smaller than the material tensile strength f that defines the tension cutoff. Material in the radially cracked region is taken as linear with $\sigma_\theta = 0$.

In the next two sections, we develop spherically symmetric cavity-expansion equations. First, we treat the target as an incompressible material and then as a compressible material. The incompressible solutions could be reasonable approximation for high-strength concrete targets (Forrestal *et al.*, 1992) or ceramic targets (Satapathy and Bless, 1995). For the concrete targets analyzed in this study, the target must be treated as a compressible material.

CAVITY-EXPANSION FOR AN INCOMPRESSIBLE MATERIAL

Elastic–plastic response

For an incompressible target, the equations of mass and momentum conservation in Eulerian coordinates for the plastic region are

$$\frac{\partial v}{\partial r}+\frac{2v}{r} = 0 \tag{2a}$$

$$\frac{\partial \sigma_r}{\partial r}+\frac{2}{r}(\sigma_r-\sigma_\theta) = -\rho_0\left(\frac{\partial v}{\partial t}+v\frac{\partial v}{\partial r}\right) \tag{2b}$$

where v is particle velocity measured positive outward, and σ_r, σ_θ are radial and circumferential Cauchy stress components taken positive in compression. Equations (1) and (2b) are combined to eliminate σ_θ, so the momentum equation becomes

$$\frac{\partial \sigma_r}{\partial r}+\frac{\alpha\lambda\sigma_r}{r}+\frac{\alpha\tau}{r} = -\rho_0\left(\frac{\partial v}{\partial t}+v\frac{\partial v}{\partial r}\right) \tag{2c}$$

where

$$\alpha = \frac{6}{3+2\lambda}. \tag{2d}$$

We define the dimensionless variables

$$S = \sigma_r/\tau, \quad U = v/c, \quad \varepsilon = V/c \tag{3a}$$

and introduces the similarity transformation

$$\xi = r/ct \tag{3b}$$

where c is the elastic–plastic interface velocity shown in Fig. 1a. With (3a, b), eqns (2a, c) transform to

$$\frac{dU}{d\xi}+\frac{2U}{\xi}=0 \tag{4a}$$

$$\frac{dS}{d\xi}+\frac{\alpha\lambda S}{\xi}=-\frac{\alpha}{\xi}+\frac{\rho_0 c^2}{\tau}\left(\xi\frac{dU}{d\xi}-U\frac{dU}{d\xi}\right). \tag{4b}$$

The boundary condition at the cavity surface is

$$U(\xi=\varepsilon)=\varepsilon. \tag{5}$$

Equation (4a) with the boundary condition (5) has solution

$$U=\varepsilon^3/\xi^2. \tag{6}$$

We substitute (6) into (4b), multiply each term by $\xi^{\alpha\lambda}$, and note that

$$\xi^{\alpha\lambda}\left[\frac{dS}{d\xi}+\alpha\lambda\frac{S}{\xi}\right]=\frac{d}{d\xi}[\xi^{\alpha\lambda}S]. \tag{7a}$$

Equation (4b) becomes

$$\frac{d}{d\xi}[\xi^{\alpha\lambda}S]=-\alpha\xi^{\alpha\lambda-1}-\frac{2\rho_0 c^2\varepsilon^3}{\tau}\cdot\xi^{\alpha\lambda-2}+\frac{2\rho_0 c^2\varepsilon^6}{\tau}\cdot\xi^{\alpha\lambda-5} \tag{7b}$$

and integrates to

$$S=-\frac{1}{\lambda}-\frac{2\rho_0 c^2\varepsilon^3}{\tau(\alpha\lambda-1)}\cdot\frac{1}{\xi}+\frac{2\rho_0 c^2\varepsilon^6}{\tau(\alpha\lambda-4)}\cdot\frac{1}{\xi^4}+C\xi^{-\alpha\lambda} \tag{7c}$$

where C is an integration constant.

Forrestal and Luk (1988) present equations for the dimensionless radial stress and particle displacement in the elastic region. Particle velocity is obtained by differentiating displacement with respect to time, and

$$S=\frac{2}{3\xi^3}+\frac{3\rho_0 c^2}{E\xi} \tag{8a}$$

$$U=\frac{3\tau}{2E\xi^2}. \tag{8b}$$

The elastic and plastic response regions are linked through the Hugoniot jump conditions that conserve mass and momentum across the elastic–plastic interface, $\xi=1$. From Hopkins (1960),

$$\rho_2(v_2-c)=\rho_1(v_1-c) \tag{9a}$$

$$\sigma_2+\rho_2 v_2(v_2-c)=\sigma_1+\rho_1 v_1(v_1-c) \tag{9b}$$

where subscripts 1 and 2 represent quantities in the elastic and plastic regions, respectively. For an incompressible material, $\rho_1=\rho_2=\rho_0$ and both radial stress and particle velocity are continuous at the interface.

From (6) and (8b), evaluated at $\xi=1$

$$\varepsilon = \frac{V}{c} = \left(\frac{3\tau}{2E}\right)^{1/3}. \tag{10}$$

We solve for the integration constant C in (7c) by equating (7c) to (8a) at $\xi = 1$, and the dimensionless radial stress in the plastic region is given by

$$S = \frac{2}{\alpha\lambda}\xi^{-\alpha\lambda} - \frac{1}{\lambda} + \frac{2\rho_0 V^2}{\tau}\left[\frac{\varepsilon}{(1-\alpha\lambda)\xi} - \frac{\varepsilon^4}{(4-\alpha\lambda)\xi^4}\right] + \frac{\rho_0 c^2}{\tau}\left[\frac{3\tau}{E} + \frac{2\varepsilon^3}{(\alpha\lambda-1)} - \frac{2\varepsilon^6}{(\alpha\lambda-4)}\right]\xi^{-\alpha\lambda}. \tag{11}$$

Our penetration models require radial stress at the cavity surface, so we write

$$S(\varepsilon) = \frac{2}{\alpha\lambda}\varepsilon^{-\alpha\lambda} - \frac{1}{\lambda} + \frac{\rho_0 V^2}{\tau}\left[\frac{6}{(1-\alpha\lambda)(4-\alpha\lambda)} - \frac{2\alpha\lambda}{1-\alpha\lambda}\varepsilon^{1-\alpha\lambda} + \frac{2\varepsilon^{4-\alpha\lambda}}{4-\alpha\lambda}\right] \tag{11b}$$

where ε is given by (10). For $V = 0$, we recover the quasi-static equation derived by Forrestal and Longcope (1990).

Elastic–cracked-plastic response

This problem has the three response regions shown in Fig. 1b. The plastic response is described by the dimensionless radial stress and dimensionless particle velocity give by (7c) and (6), respectively. However, the cracked region has $\sigma_\theta = \sigma_\phi = 0$, so radial stress at the cracked-plastic interface is the unconfined compressive strength Y. Thus,

$$S(\xi = 1) = Y/\tau. \tag{12}$$

Evaluating the constant C in (7c) with (12) gives

$$S = \left[\frac{3+2\lambda}{\lambda(3-\lambda)}\right]\xi^{-\alpha\lambda} - \frac{1}{\lambda} - \frac{2\rho_0 c^2}{\tau}\left[\frac{\varepsilon^3}{(\alpha\lambda-1)\xi} - \frac{\varepsilon^6}{(\alpha\lambda-4)\xi^4}\right] + \frac{2\rho_0 c^2}{\tau}\left[\frac{\varepsilon^3}{\alpha\lambda-1} - \frac{\varepsilon^6}{\alpha\lambda-4}\right]\xi^{-\alpha\lambda}. \tag{13}$$

The cracked region in Fig. 1b is taken as incompressible and linear. Thus, the mass conservation is given by (2a). However, for momentum conservation, we set $\sigma_\theta = 0$ and neglect the convective term in (2b). The dimensionless momentum equation for the cracked region is

$$\frac{\mathrm{d}S}{\mathrm{d}\xi} + \frac{2S}{\xi} = \frac{\rho_0 c^2}{\tau}\cdot\xi\frac{\mathrm{d}U}{\mathrm{d}\xi}. \tag{14}$$

For convenience, we define

$$\beta = c/c_y, \quad \beta_1 = c_1/c_y, \quad c_y^2 = \tau/\rho_0 \tag{15}$$

where c is the cracked-plastic interface velocity and c_1 is the elastic-cracked interface velocity shown in Fig. 1b.

As before, we solve (4a) for U, substitute U into (14), and solve for S. We obtain

$$U = \frac{A}{\xi^2} \tag{16a}$$

$$S = \frac{B}{\xi^2} - \frac{2A\beta^2}{\xi} \tag{16b}$$

where A and B are integration constants to be found from the interface conditions. At the cracked-plastic interface $\sigma_r(\xi = 1) = Y$, so $S(\xi = 1) = Y/\tau$. At the elastic-cracked interface $r = c_1 t$ or $\xi = \beta_1/\beta$, the radial stress is denoted as S_3. Using the radial stress interface conditions to obtain A and B, dimensionless particle velocity and radial stress in the cracked region are given by

$$U = \frac{1}{2\beta^2}\left\{\frac{(\beta/\beta_1)^2(Y/\tau) - S_3}{(\beta/\beta_1)[1-(\beta/\beta_1)]}\right\}\frac{1}{\xi^2} \tag{17a}$$

$$S = \left\{\frac{S_3 - (\beta/\beta_1)^2(Y/\tau)}{(\beta/\beta_1)[1-(\beta/\beta_1)]}\right\}\frac{1}{\xi} + \left\{\frac{(\beta/\beta_1)(Y/\tau) - S_3}{(\beta/\beta_1)[1-(\beta/\beta_1)]}\right\}\frac{1}{\xi^2} \tag{17b}$$

where at this point in the analysis β, β_1, and S_3 are unknown.

The elastic region in Fig. 1b is taken as linear elastic. From Forrestal and Luk (1988), the dimensionless radial stress, particle velocity, and displacement in the elastic region are given by

$$S = \frac{4DE}{3\tau\xi^3} + \frac{6D\beta^2}{\xi} \tag{18a}$$

$$U = \frac{3D}{\xi^2} \tag{18b}$$

$$\bar{u} = \frac{u}{ct} = \frac{D}{\xi^2} \tag{18c}$$

where D is an integration constant and β is defined by (15). At the elastic-cracked interface $\xi = \beta_1/\beta$, the material in the elastic region reaches its circumferential tensile strength or $\sigma_\theta = -f$. In dimensionless terms

$$\frac{\sigma_\theta}{\tau} = \frac{-f}{\tau} = -F \quad \text{at } \xi = \beta_1/\beta. \tag{19}$$

We solve for the integration constant D from Hooke's law for an incompressible material (Hill, 1950) given by

$$\sigma_r - \sigma_\theta = \frac{2Eu}{r}. \tag{20a}$$

From (3a, b), (18a, c), and (20a) we obtain

$$-\frac{\sigma_\theta}{\tau} = \frac{D}{\xi}\left[\frac{2E}{3\tau\xi^2} - 6\beta^2\right]. \tag{20b}$$

At the elastic-cracked interface $\xi = \beta_1/\beta$ in the elastic region, we use (19) and (20b) to obtain

$$D = \frac{(\beta_1/\beta)F}{\left[\dfrac{2E}{3\tau(\beta_1/\beta)^2} - 6\beta^2\right]}. \tag{21}$$

Radial stress and particle velocity in the elastic region at the elastic-cracked interface are denoted by S_3, U_3, respectively, and given by

$$S_3 = \frac{2F(2E/3\tau + 3\beta_1^2)}{(2E/3\tau - 6\beta_1^2)} \tag{22a}$$

$$\beta U_3 = \frac{3F\beta_1}{2E/3\tau - 6\beta_1^2}. \tag{22b}$$

We now present a solution procedure for the incompressible, elastic-cracked-plastic, cavity-expansion problem. As can be observed from the Hugoniot jump condition (9a, b), both radial stress and particle velocity are continuous at the interfaces for an incompressible material. Equating dimensionless particle velocities at the elastic-cracked interface $\xi = \beta_1/\beta$, we obtained quadratic equation for β, and obtain

$$\beta = \beta_1^3\left(\frac{\tau}{Y}\right)\left\{\left[\frac{2F}{\beta_1^4}\left(\frac{Y}{\tau}\right)\left(\frac{E+9\tau\beta_1^2}{E-9\tau\beta_1^2}\right)\right] + \left[\frac{9F}{2}\left(\frac{\tau}{E-9\tau\beta_1^2}\right)\right]^2\right\}^{1/2} - \frac{9\beta_1^3}{2}\left(\frac{\tau}{Y}\right)F\left(\frac{\tau}{E-9\tau\beta_1^2}\right). \tag{23a}$$

Now we equate dimensionless particle velocities at the cracked-plastic interface and obtain

$$\varepsilon^3 = \frac{1}{2\beta^2}\left\{\frac{(\beta/\beta_1)^2(Y/\tau) - S_3}{(\beta/\beta_1)[1-(\beta/\beta_1)]}\right\} \tag{23b}$$

where S_3 is given by (22a). To calculate radial stress in the plastic region (13), we must know $\varepsilon = V/c$. An explicit solution for ε is not obtainable. However, we can conveniently calculate ε with an inverse procedure. First, choose a value for β_1 and calculate β from (23a). Second, with β_1 and β now known, calculate ε from (23b). Note from eqns (3a) and (15) that $\beta\varepsilon = V/c_y$, so with this procedure, we can calculate and plot $\beta_1 = c_1/c_y$ and $\beta = c/c_y$ vs $\beta\varepsilon = V/c_y$. That is, we present an inverse procedure to calculate the interface velocities c_1, c as a function of the cavity-expansion velocity V.

Our penetration models require radial stress at the cavity surface, so we write

$$S(\varepsilon) = \left[\frac{3+2\lambda}{\lambda(3-\lambda)}\right]\varepsilon^{-\alpha\lambda} - \frac{1}{\lambda} + \frac{6}{(\alpha\lambda-1)(\alpha\lambda-4)}\left(\frac{\rho_0 V^2}{\tau}\right) + 2\left(\frac{\rho_0 V^2}{\tau}\right)\left(\frac{\varepsilon}{\alpha\lambda-1} - \frac{\varepsilon^4}{\alpha\lambda-4}\right)\varepsilon^{-\alpha\lambda} \tag{24}$$

where $\varepsilon = V/c$. In the previous paragraph, we present an inverse procedure to calculate the cracked-plastic interface velocity c as a function of V. Thus, we can also calculate $S(\varepsilon)$ as a function of V.

CAVITY-EXPANSION FOR A COMPRESSIBLE MATERIAL

Elastic–plastic response

For a compressible target, the equations of mass and momentum conservation in Eulerian coordinates for the plastic region are

$$\rho\left(\frac{\partial v}{\partial r}+\frac{2v}{r}\right)=-\left(\frac{\partial \rho}{\partial t}+v\frac{\partial \rho}{\partial r}\right) \tag{25a}$$

$$\frac{\partial \sigma_r}{\partial r}+\frac{2(\sigma_r-\sigma_\theta)}{r}=-\rho\left(\frac{\partial v}{\partial t}+v\frac{\partial v}{\partial r}\right) \tag{25b}$$

where v is the particle velocity taken as positive outward and other terms are defined under (1a–1c). Equations (1, 25) are combined to eliminate σ_θ and ρ, so we obtain two equations in σ_r and v.

$$\frac{\partial v}{\partial r}+\frac{2v}{r}=-\frac{\alpha}{2K(1-\eta)}\left(\frac{\partial \sigma_r}{\partial t}+v\frac{\partial \sigma_r}{\partial r}\right) \tag{26a}$$

$$\frac{\partial \sigma_r}{\partial r}+\frac{\alpha\lambda\sigma_r}{r}+\frac{\alpha\tau}{r}=-\frac{\rho_0}{1-\eta}\left(\frac{\partial v}{\partial t}+v\frac{\partial v}{\partial r}\right) \tag{26b}$$

$$\alpha=6/(3+2\lambda) \tag{26c}$$

$$\eta=\frac{\alpha\tau}{2K}\left(\frac{\sigma_r}{\tau}-\frac{2}{3}\right). \tag{26d}$$

We introduce the dimensionless variables†

$$S=\sigma_r/\tau,\quad U=v/c,\quad \varepsilon=V/c,\quad \beta=c/c_p,\quad \beta_1=c_1/c_p,\quad \beta\varepsilon=V/c_p,\quad c_p^2=K/\rho_0 \tag{27a}$$

and the similarity transformation

$$\xi=r/ct. \tag{27b}$$

With (27a, b), (26a, b) transform to

$$\frac{\mathrm{d}U}{\mathrm{d}\xi}+\frac{2U}{\xi}=\frac{\tau\alpha}{2K(1-\eta)}\cdot(\xi-U)\frac{\mathrm{d}S}{\mathrm{d}\xi} \tag{28a}$$

$$\frac{\mathrm{d}S}{\mathrm{d}\xi}+\alpha\lambda\frac{S}{\xi}+\frac{\alpha}{\xi}=\frac{\beta^2K}{\tau(1-\eta)}\cdot(\xi-U)\frac{\mathrm{d}U}{\mathrm{d}\xi} \tag{28b}$$

$$\eta=\frac{\alpha\tau}{2K}\left(S-\frac{2}{3}\right). \tag{28c}$$

The boundary condition at the cavity surface is

$$U(\xi=\varepsilon)=\varepsilon. \tag{29}$$

We put the coupled eqns (28a, b) in standard forms suitable for numerical evaluation with the Runge–Kutta method (Press *et al.*, 1989).

† Note that the dimensionless interface velocities β and β_1 are different from those defined for the incompressible analyses given by (15).

$$\frac{dU}{d\xi} = \frac{\dfrac{2U}{\xi} + \dfrac{\tau\alpha^2}{2K\xi}\left(\dfrac{\xi - U}{1-\eta}\right)(\lambda S + 1)}{\dfrac{\alpha\beta^2}{2}\left(\dfrac{\xi - U}{1-\eta}\right)^2 - 1} \tag{30a}$$

$$\frac{dS}{d\xi} = \frac{\dfrac{\alpha}{\xi} + \dfrac{\alpha\lambda S}{\xi} + \dfrac{2\beta^2 KU}{\tau\xi}\left(\dfrac{\xi - U}{1-\eta}\right)}{\dfrac{\alpha\beta^2}{2}\left(\dfrac{\xi - U}{1-\eta}\right)^2 - 1} \tag{30b}$$

where η is given by (28c). We define dimensionless radial stress and dimensionless particle velocity in the plastic region at the elastic–plastic interface as

$$S(\xi = 1) = S_2, \quad U(\xi = 1) = U_2 \tag{31}$$

where S_2 and U_2 are later determined from the elastic response and the Hugoniot jump conditions that conserve mass and momentum across the elastic–plastic interface. Once S_2 and U_2 are found, the calculation proceeds from the elastic–plastic interface $\xi = 1$ to the cavity surface $\xi = \varepsilon$.

The elastic and plastic response regions are linked through the Hugoniot jump conditions (9a, b). In dimensionless form

$$U_2 = 1 - (\rho_1/\rho_2)(1 - U_1) \tag{32a}$$

$$S_2 = S_1 + \beta^2(K/\tau)(\rho_1/\rho_0)(U_2 - U_1)(1 - U_1) \tag{32b}$$

where subscript 1 refers to quantities in the elastic region at $\xi = 1$ and subscript 2 refers to quantities in the plastic region at $\xi = 1$. The Mohr–Coulomb yield criterion applies on either side of the elastic–plastic interface, so the dimensionless radial interface stresses are

$$S_1 = (2K/\alpha\tau)(1 - \rho_0/\rho_1) + 2/3 \tag{32c}$$

$$S_2 = (2K/\alpha\tau)(1 - \rho_0/\rho_2) + 2/3. \tag{32d}$$

Eliminating ρ_1 and ρ_2 from (32a–d) shows there are no jumps in radial stress or particle velocity across the interface. Thus

$$U_2 = U_1, \quad S_2 = S_1 \tag{33}$$

and $\rho_1 = \rho_2$ at $\xi = 1$ from (32c, d).

Forrestal and Luk (1988) present response equations for the elastic region. However, the constant in this general solution depends on the yield criterion at the elastic–plastic interface or the tensile strength at the elastic-cracked interface. For the elastic–plastic problem, the constant is determined from the elastic equations for radial and circumferential stresses evaluated at the elastic–plastic interface $\xi = 1$ with the Mohr–Coulomb yield criterion given by (1c). In addition, radial stress and particle velocity are continuous at the elastic–plastic interface. Thus, dimensionless radial stress and dimensionless particle velocity at $\xi = 1$ are

$$S_1 = S_2 = \frac{2[(1-2\nu)(1+\gamma\beta) + (1+\nu)(\gamma\beta)^2]}{3(1-2\nu)(1+\gamma\beta) - 2\lambda(1+\nu)(\gamma\beta)^2} \tag{34a}$$

$$U_1 = U_2 = \frac{3\tau(1+\nu)(1-2\nu)(1+\gamma\beta)}{E[3(1-2\nu)(1+\gamma\beta) - 2\lambda(1+\nu)(\gamma\beta)^2]} \tag{34b}$$

$$\gamma^2 = \left(\frac{c_p}{c_d}\right)^2 = \frac{1+\nu}{3(1-\nu)}, \quad c_d^2 = \frac{E(1-\nu)}{(1+\nu)(1-2\nu)\rho_0}. \tag{34c}$$

For numerical evaluation, we select a value of $\beta = c/c_p$ and solve for S_2 and U_2 given by (34a, c). With S_2 and U_2 known, we can calculate dimensionless radial stress and particle velocity in the plastic region with (30a, b). The calculation proceeds from the elastic–plastic interface $\xi = 1$ to the cavity surface $\xi = \varepsilon$. When the particle velocity boundary condition at the cavity surface given by (29) is satisfied, we obtain the value of $\varepsilon = V/c$ corresponding to the chosen value of $\beta = c/c_p$. Since $\beta\varepsilon = V/c_p$, we can find the value of V/c_p corresponding to the chosen value of $\beta = c/c_p$. Thus, we present an inverse procedure to calculate the interface velocity $c(\beta = c/c_p)$ vs the cavity-expansion velocity $V(\beta\varepsilon = V/c_p)$. In addition, we also calculate the dimensionless radial stress S vs the cavity-expansion velocity V.

Elastic–cracked-plastic response

This problem has the three response regions shown in Fig. 1b. We have already presented solution procedures for the plastic response region. However, the elastic–plastic solution depended on the dimensionless radial stress and particle velocity at the elastic–plastic interface given by (34a, b). To determine the dimensionless radial stress in the plastic region for this elastic–cracked-plastic problem, we must now find the dimensionless radial stress and particle velocity at the cracked-plastic interface $\xi = 1$. To obtain these equations, we solve for the responses in the elastic and cracked regions and link these regions with the Hugoniot jump conditions (9a, b).

As shown in Fig. 1b, the elastic region is bounded by $r = c_1 t$ and $r = c_d t$ where c_1 is the elastic-cracked interface velocity and c_d is the elastic dilatational velocity. In dimensionless coordinates the elastic region is bounded by $\xi = \beta_1/\beta$ and $\xi = 1/\gamma\beta$. Forrestal and Luk (1988) present response equations for the elastic region. However, the constant in this general solution depends on the circumferential tensile strength at the elastic-cracked interface β_1/β. Thus,

$$\frac{\sigma_\theta}{\tau} = -\frac{f}{\tau} = -F \quad \text{at } \xi = \beta_1/\beta \tag{35}$$

where f is tensile strength. The dimensionless radial stress and particle velocity in the elastic region at the elastic-cracked interface are

$$S_3 = 2F\left[\frac{(1-2\nu)+3\nu(\gamma\beta_1)^2-(1+\nu)(\gamma\beta_1)^3}{1-2\nu-3(\gamma\beta_1)^2+2(1+\nu)(\gamma\beta_1)^3}\right] \tag{36a}$$

$$\beta U_3 = \frac{3(1+\nu)(1-2\nu)\tau F\beta_1}{E}\left[\frac{1-(\gamma\beta_1)^2}{(1-2\nu)-3(\gamma\beta_1)^2+2(1+\nu)(\gamma\beta_1)^3}\right] \tag{36b}$$

where $S_3(\beta_1)$ and $\beta U_3(\beta_1)$.

Figure 1b shows that the radially cracked region is bounded by $r = ct$ and $r = c_1 t$ where c and c_1 are the cracked-plastic and elastic-cracked interface velocities, respectively. In dimensionless coordinates the cracked region is bounded by $\xi = 1$ and $\xi = \beta_1/\beta$. Material in the cracked region is taken as linear and compressible with $\sigma_\theta = 0$. Neglecting the convective terms in (25a, b) and setting $\sigma_\theta = 0$, the equations of mass and momentum conservation for the radially cracked region are

$$\frac{dU}{d\xi} + \frac{2U}{\xi} = \frac{\tau}{3K}\cdot\xi\frac{dS}{d\xi} \tag{37a}$$

$$\frac{dS}{d\xi} + \frac{2S}{\xi} = \frac{\beta^2 K}{\tau}\cdot\xi\frac{dU}{d\xi}. \tag{37b}$$

We solve eqns (37a, b) for U and S by obtaining an equation in S only. From (37a, b)

$$\left(1-\frac{\beta^2\xi^2}{3}\right)\frac{d^2S}{d\xi^2}+\left(\frac{4}{\xi}-\frac{2\beta^2\xi}{3}\right)\frac{dS}{d\xi}+\frac{2S}{\xi^2}=0 \tag{38a}$$

which has solution

$$S(\xi)=\frac{C}{\beta\xi}+D\left[1+\frac{3}{(\beta\xi)^2}\right] \tag{38b}$$

where C and D are integration constants. Next, we substitute (38b) into (37b) and solve for U. An integration gives

$$U(\xi)=\frac{-\tau}{2K\beta}\left[\frac{C}{3}+\frac{C}{(\beta\xi)^2}+\frac{4D}{\beta\xi}\right]. \tag{38c}$$

The three response regions shown in Fig. 1b are linked through the Hugoniot jump conditions (9a, b) or given in dimensionless form by (32a, b). For application to the cracked-plastic interface, subscripts 1 refer to quantities in the cracked region at $\xi = 1$ and subscripts 2 refer to quantities in the plastic region at $\xi = 1$. The Mohr–Coulomb yield criterion applies on either side of the cracked-plastic interface, so the dimensionless radial stresses are given by (32c, d). In the cracked region at $\xi = 1$, $\sigma_r = Y$, or the radial stress equals the unconfined compression stress, so (32c) becomes

$$S_1=\frac{3K}{\tau}\left(1-\frac{\rho_0}{\rho_1}\right)=\frac{Y}{\tau}. \tag{39}$$

Eliminating ρ_1 and ρ_2 from (32a–c) and (39) shows that there are no jumps in radial stress or particle across the cracked-plastic interface. Thus,

$$U_2 = U_1, \quad S_2 = S_1 \tag{40}$$

For the Hugoniot jump conditions at the elastic-cracked interface $\xi = \beta_1/\beta$ shown in Fig. 1b, we use subscripts 3 to denote quantities in the elastic region at $\xi = \beta_1/\beta$ and subscript 4 to denote quantities in the cracked region at $\xi = \beta_1/\beta$. The dimensionless Hugoniot jump condition for the elastic-cracked interface are

$$U_4=\frac{\beta_1}{\beta}-\frac{\rho_3}{\rho_4}\left(\frac{\beta_1}{\beta}-U_3\right) \tag{41a}$$

$$S_4=S_3+\frac{\rho_3\beta^2K}{\rho_0\tau}\left(\frac{\beta_1}{\beta}-U_3\right)(U_4-U_3). \tag{41b}$$

The dimensionless radial stresses at the elastic-cracked interface are

$$S_3=\frac{3K}{\tau}\left(1-\frac{\rho_0}{\rho_3}\right)+2F \tag{41c}$$

$$S_4=\frac{3K}{\tau}\left(1-\frac{\rho_0}{\rho_4}\right). \tag{41d}$$

We now eliminate ρ_3, ρ_4 from (41a–d) to obtain the dimensionless particle velocity and radial stress in the cracked region at the elastic-cracked interface. Thus,

$$\beta U_4 = \beta U_3 + \frac{(2f/3K)(\beta_1 - \beta U_3)(1 + 2f/3K - \tau S_3/3K)}{(1 + 2f/3K - \tau S_3/3K)^2 - (\beta_1 - \beta U_3)^2/3} \tag{42a}$$

$$S_4 = S_3 + \frac{(2f/3\tau)(\beta_1 - \beta U_3)^2}{(1 + 2f/3K - \tau S_3/3K)^2 - (\beta_1 - \beta U_3)^2/3}. \tag{42b}$$

For our application both $(2f/3K)$ and $(\tau S_3/3K)$ are small compared with unity, and (42a, b) can be approximated accurately with

$$\beta U_4 = \beta U_3 + \frac{(2f/K)(\beta_1 - \beta U_3)}{3 - (\beta_1 - \beta U_3)^2} \tag{43a}$$

$$S_4 = S_3 + \frac{2F(\beta_1 - \beta U_3)^2}{3 - (\beta_1 - \beta U_3)^2}. \tag{43b}$$

As previously discussed, we evaluate the plastic response region numerically with the Runge–Kutta method that requires both the dimensionless particle velocity and radial stress at the cracked-plastic interface in the plastic region. We proved that both radial stress and particle velocity are continuous at the cracked-plastic interface (40). Also, the radial stress in the cracked region at the cracked-plastic interface is $\sigma_r = Y$, where Y is the unconfined compressive strength. Thus

$$S_1 = S_2 = Y/\tau. \tag{44}$$

Particle velocity at the cracked-plastic interface $U_1 = U_2$ is found with an inverse procedure that uses the equations for the elastic and cracked regions and the Hugoniot jump conditions that link these regions. To solve for U_2, we choose a value of β_1 and calculate S_3 and βU_3 from (36a, b). Next, calculate S_4 and βU_4 from (43a, b). Solving for the integration constants in the equations for the cracked region (38b, c) with the boundary conditions at the elastic-cracked interface $\xi = \beta_1/\beta$ (43a, b) gives

$$C = \frac{-6\beta_1^2[2\beta_1 \tau S_4 + (\beta_1^2 + 3)K(\beta U_4)]}{\tau(\beta_1^2 - 3)^2} \tag{45a}$$

$$D = \frac{\beta_1^2[\tau S_4(\beta_1^2 + 3) + 6\beta_1 K(\beta U_4)]}{\tau(\beta_1^2 - 3)^2}. \tag{45b}$$

At the cracked-plastic interface $\xi = 1$, we use (38b) and (44) to obtain

$$\frac{Y}{\tau} = \frac{C}{\beta} + D\left(1 + \frac{3}{\beta^2}\right). \tag{46}$$

We put (46) in the standard form for a quadratic equation in β, and obtain

$$\beta = \frac{C + [C^2 + 12D(Y/\tau - D)]^{1/2}}{2(Y/\tau - D)}. \tag{47}$$

At the cracked-plastic interface $\xi = 1$, particle velocity is continuous, so from (38c)

$$U_2 = \frac{-\tau(\beta^2 + 3)C}{6K\beta^3} - \frac{2\tau D}{K\beta^2}. \tag{48}$$

As previously discussed, particle velocity at the cracked-plastic interface U_2 must be

found to calculate radial stress in the plastic region. As explicit solution for U_2 is not obtainable, so we present an inverse procedure. First select a value of β_1 and calculate β from (36, 43, 45, and 47). Next, calculate U_2 from (48). For these values of β_1, β, U_2, and S_2 given by (44), we calculate particle velocity and radial stress in the plastic region from (30a, b). The calculation proceeds from the cracked-plastic interface $\xi = 1$ to the cavity surface $\xi = \varepsilon$. When the particle velocity boundary condition at the cavity surface given by (29) is satisfied, we obtain the value of $\varepsilon = V/c$ corresponding to the chosen value of $\beta = c/c_p$. Since $\beta\varepsilon = V/c_p$, we find the value of V/c_p corresponding to the chosen values of $\beta_1 = c_1/c_p$ and $\beta = c/c_p$. Thus, we present an inverse procedure to calculate the interface velocities vs the cavity-expansion velocity. In addition, we also calculate the dimensionless radial stress S vs the cavity-expansion velocity V.

CAVITY-EXPANSION NUMERICAL RESULTS

We present numerical results for a concrete material for which we have both triaxial material test data† (Joy and Ehrgott, 1993) and depth of penetration data (Forrestal *et al.*, 1996). Figure 2 shows data and linear curve fits for pressure vs volumetric strain and shear strength vs confining pressure. For input to our cavity-expansion equations we take

$K = 6.7$ GPa, $Y = 130$ MPa, $\lambda = 0.67$, $E = 11.3$ GPa, $\nu = 0.22$, $f = 13$ MPa, and $\rho_0 = 2260$ kg/m^3.

Figures 3 and 4 show predictions from the compressible, elastic–plastic model with the concrete input parameters for $0 < V/(Y/\rho_0)^{1/2} < 7.0$, which corresponds to $0 < V < 1680$ m/s. Our compressible, elastic–plastic model assumes the response regions shown in Fig. 1a, so the cavity-expansion velocity V must be less than the elastic–plastic interface velocity c. For large values of V, the interface velocity c approaches $[(1+2\lambda/3)(K/\rho_0)]^{1/2}$, which is the interface velocity for the compressible, one-dimensional strain problem (Chou and Hopkins, 1972). Figure 3 shows that the dimensionless interface velocity $c/(Y/\rho_0)^{1/2}$ approaches 8.62, which corresponds to an elastic–plastic interface velocity of $c = 2070$ m/s. In addition, the interface velocity c must be less than the elastic dilatational velocity c_d. For this concrete material, $c_d = 2390$ m/s. So the results shown in Figs 3 and 4 for the compressible, elastic–plastic model do not violate the model assumptions shown in Fig. 1a.

Figure 3 shows predictions for the elastic–plastic interface velocity vs cavity-expansion velocity. For an incompressible material, eqn (10) gives a linear relationship between c and V; whereas for a compressible material, the interface velocity approaches a constant value as the cavity-expansion velocity increases. As previously mentioned, c approaches the interface velocity for the compressible, one-dimensional strain problem. Figure 4 shows predictions for the radial stress at the cavity surface vs cavity-expansion velocity for an incompressible and a compressible material. For cavity-expansion velocity V approaching zero, we obtained numerical values for radial stress corresponding to the quasi-static solutions derived by Forrestal and Longcope (1990).

We show later that the cavity-expansion results are used as input to our penetration equations. For this study, we analyze projectile penetration for striking velocities to 1100 m/s and require cavity-expansion results to $V/(Y/\rho_0)^{1/2} = 2.5$. So the dimensionless range for Figs 5–8 are presented for $0 < V/(Y/\rho_0)^{1/2} < 3.0$. Figures 5 and 6 show predictions for an incompressible material from the elastic–plastic and elastic–cracked-plastic models. For the elastic–cracked-plastic model (Fig. 1b), the elastic-cracked interface velocity c_1 is greater than the cracked-plastic interface velocity c until $V/(Y/\rho_0)^{1/2} = 0.71$. For $V/(Y/\rho_0)^{1/2} > 0.71$, the radially cracked region is eliminated and the response is elastic–plastic. Figures 7 and 8 show predictions for a compressible material from the elastic–plastic and elastic–cracked-plastic models. For the elastic–cracked-plastic model (Fig. 1b), the elastic-cracked interface velocity c_1 is greater than the cracked-plastic interface velocity c until $V/(Y/\rho_0)^{1/2} = 1.7$. For $V/(Y/\rho_0)^{1/2} > 1.7$, the radially cracked region is eliminated and the response is elastic–plastic. When the cavity-expansion velocity V approaches zero in Figs 6 and 8, we obtain

† Mellegard *et al.* (1993) describe procedures for triaxial material tests.

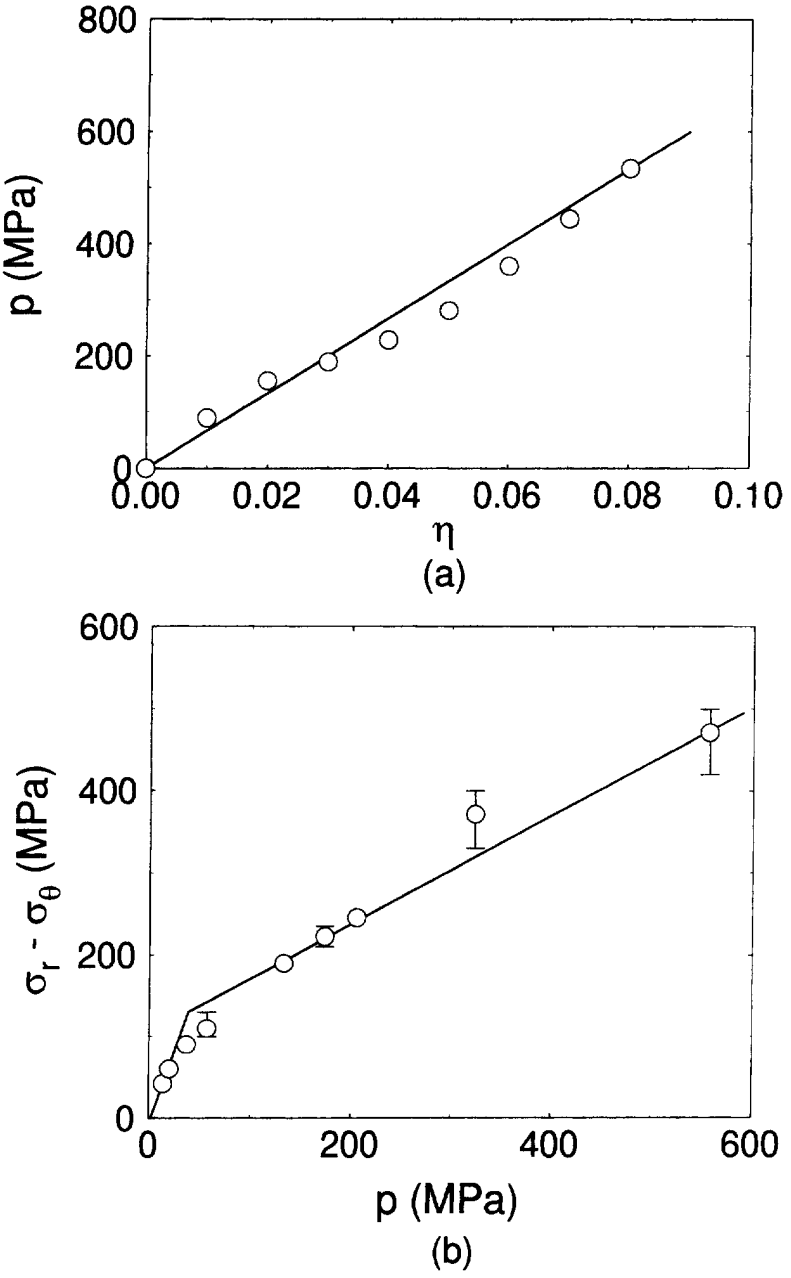

Fig. 2. Material data and constitutive idealizations: (a) pressure vs volumetric strain and (b) shear strength vs pressure.

numerical values for radial stress corresponding to the quasi-static solutions derived by Forrestal and Longcope (1990).

PENETRATION EQUATIONS AND COMPARISON OF PREDICTIONS WITH DATA

Our penetration equations use the spherical cavity-expansion approximation introduced by Bishop *et al.* (1945), Goodier (1965), and modified by Forrestal *et al.* (1995). To obtain closed-form penetration equations, we curve-fit the numerical results from the spherically symmetric cavity-expansion models with

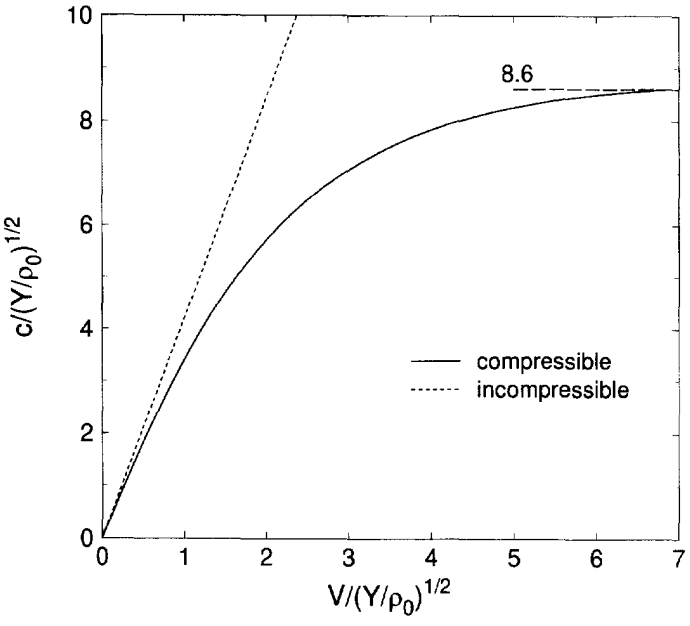

Fig. 3. Elastic–plastic interface velocity vs cavity-expansion velocity for the incompressible and compressible elastic–plastic materials.

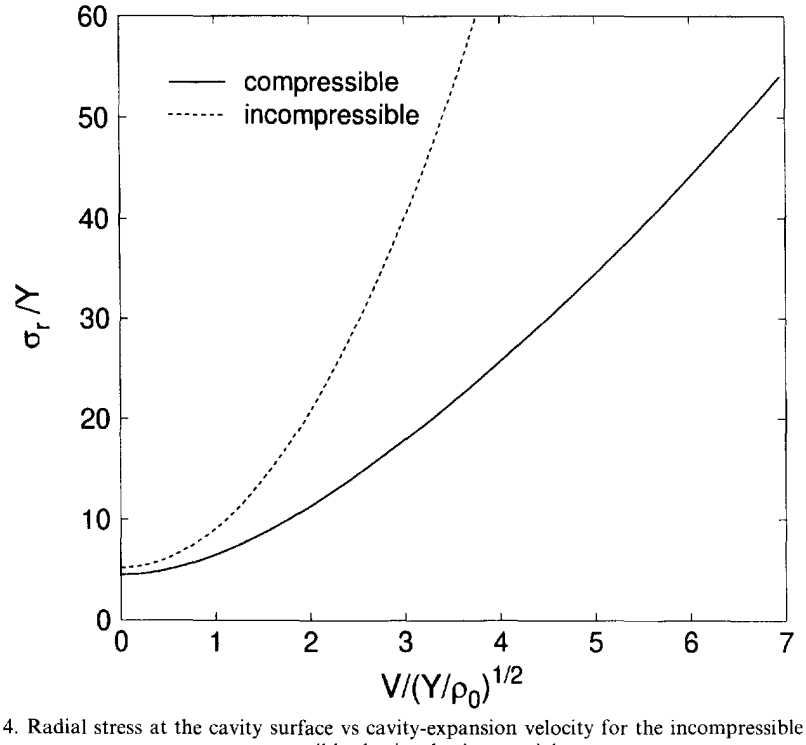

Fig. 4. Radial stress at the cavity surface vs cavity-expansion velocity for the incompressible and compressible elastic–plastic materials.

$$\frac{\sigma_r}{Y} = A + B\left[\frac{V}{(Y/\rho_0)^{1/2}}\right] + C\left[\frac{V}{(Y/\rho_0)^{1/2}}\right]^2 \tag{49}$$

where A, B, and C are dimensionless. Forrestal and Longcope (1990) give equations for the quasi-static response, so A is determined and only the coefficients B and C are used for

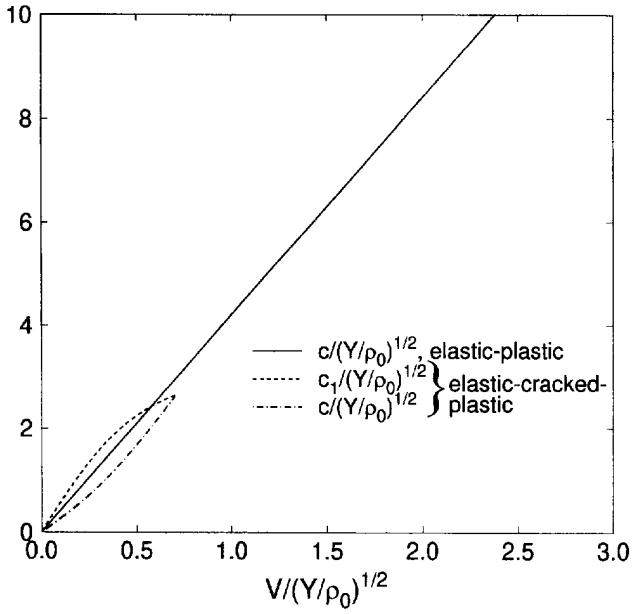

Fig. 5. Interface velocities vs cavity-expansion velocity for the incompressible material.

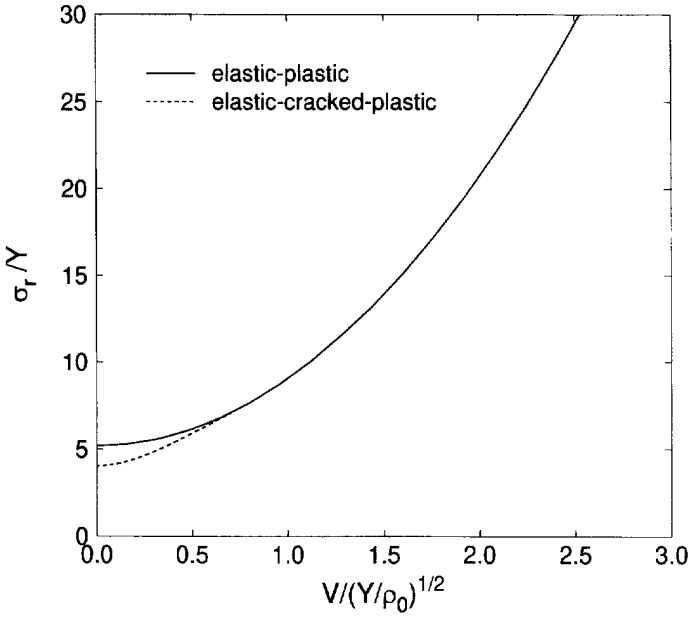

Fig. 6. Radial stresses at the cavity surface vs cavity-expansion velocity for the incompressible material.

the curve-fits. Values of A, B, and C for the four, spherically symmetric cavity-expansion models are listed in Table 1 and accurately fit the results shown in Figs 6 and 8.

Using the procedures published by Forrestal *et al.* (1992) and Forrestal *et al.* (1994), final depth of penetration P is given by

$$P = \frac{m}{2\pi a^2 C N_2 \rho_0}\left\{ln\left[1+\frac{BN_1}{A}\left(\frac{\rho_0}{Y}\right)^{1/2}V_1+\frac{CN_2\rho_0 V_1^2}{AY}\right]\right.$$
$$\left.+\frac{2BN_1}{D}\left[\tan^{-1}\left(\frac{BN_1}{D}\right)-\tan^{-1}\left(\frac{2CN_2(\rho_0/Y)^{1/2}V_1+BN_1}{D}\right)\right]\right\}+4a, \quad P>4a \tag{50}$$

where

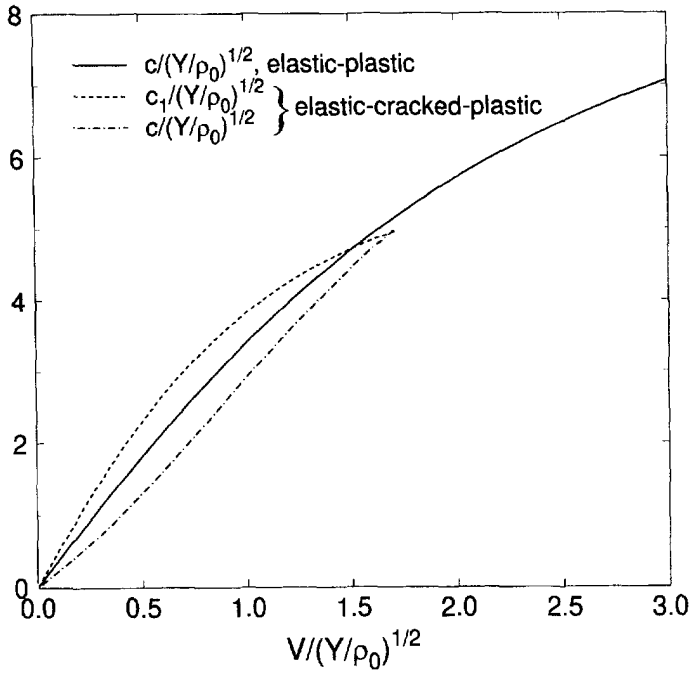

Fig. 7. Interface velocities vs cavity-expansion velocity for the compressible material.

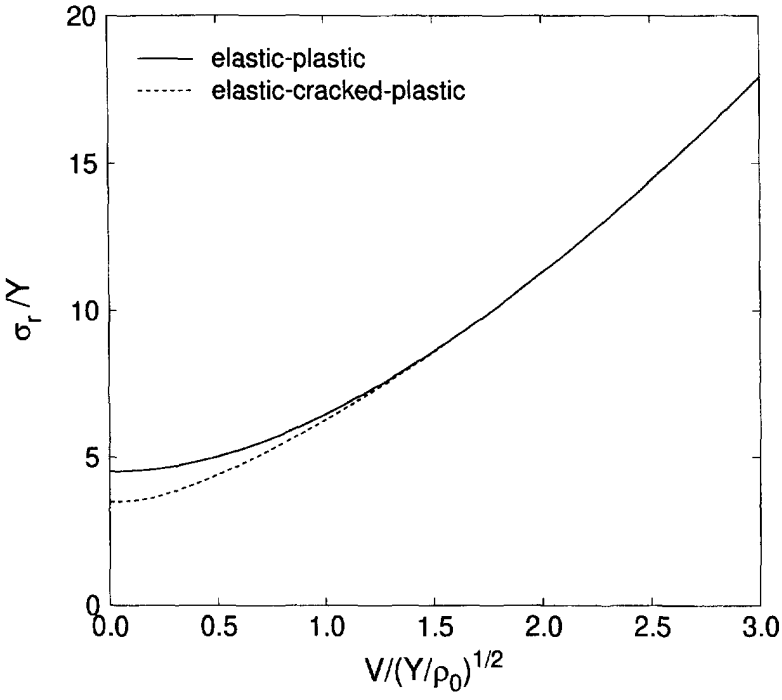

Fig. 8. Radial stresses at the cavity surface vs cavity-expansion velocity for the compressible material.

$$D = [4ACN_2 - (BN_1)^2]^{1/2} \tag{51a}$$

$$N_1(\psi) = \frac{(4\psi-1)^{3/2}}{3\psi} + \frac{(2\psi-1)^2(4\psi-1)^{1/2}}{2\psi} - \psi(2\psi-1)(\pi-2\theta_0) \tag{51b}$$

$$\theta_0 = \sin^{-1}\left(\frac{2\psi-1}{2\psi}\right) \tag{51c}$$

Table 1. Curve-fit parameters. Model 1—incompressible, elastic–plastic; Model 2—incompressible, elastic–cracked-plastic; Model 3—compressible, elastic–plastic; Model 4—compressible, elastic–cracked-plastic

Model	A	B	C
1	5.18	0	3.88
2	4.05	1.36	3.51
3	4.50	0.75	1.29
4	3.45	1.60	1.12

$$N_2(\psi) = \frac{8\psi - 1}{24\psi^2} \tag{51d}$$

and V_1 is obtained from

$$\left[\frac{m}{4\pi a^3 Y} + \frac{CN_2}{(Y/\rho_0)}\right] V_1^2 + \frac{BN_1}{(Y/\rho_0)^{1/2}} \cdot V_1 + \left[A - \frac{mV_s^2}{4\pi a^3 Y}\right] = 0. \tag{52}$$

For (50, 51, and 52) the ogive-nose projectile is described by mass m, shank diameter $2a$, and caliber-radius-head ψ. V_s is the striking velocity and other terms were previously defined.

Forrestal *et al.* (1996) present penetration depth P vs striking velocity V_s data for an ogive-nose rod projectile with $m = 1.60$ kg, $2a = 30.5$ mm, and $\psi = 3.0$. We compare penetration depth data with model prediction for an incompressible material in Fig. 9 and for a compressible material in Fig. 10. Comparison of Figs 9 and 10 shows that material compressibility must be included for reasonable predictions. Figure 9 and 10 also compare the elastic–plastic and elastic–cracked-plastic models and show the effect of material tensile strength. The compressible, elastic–cracked-plastic model prediction shown in Fig. 10 and penetration data are in good agreement for $V_s < 800$ m/s. For $800 < V_s < 1100$ m/s, the model predicts slightly lower penetration depths than the data. We also point out that the

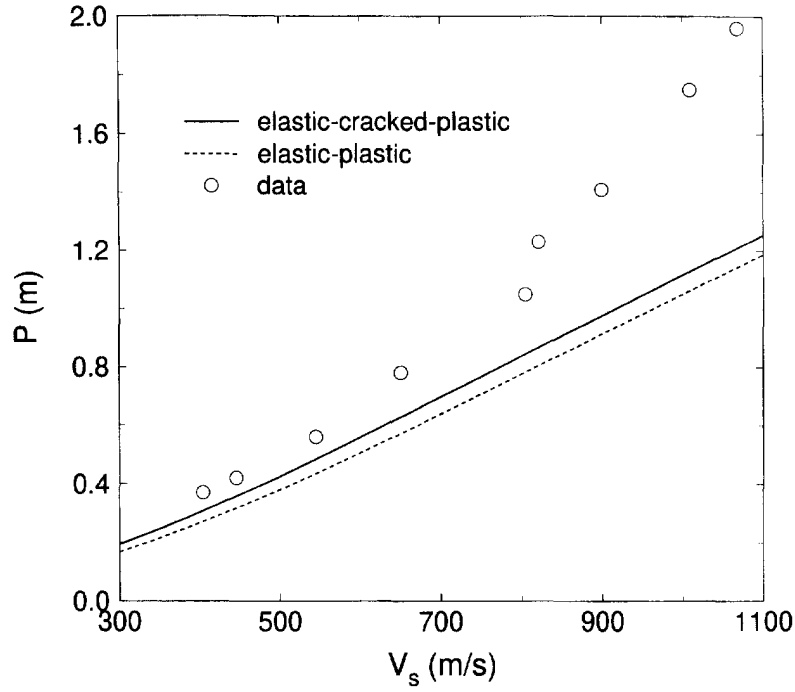

Fig. 9. Depth of penetration data and incompressible model predictions.

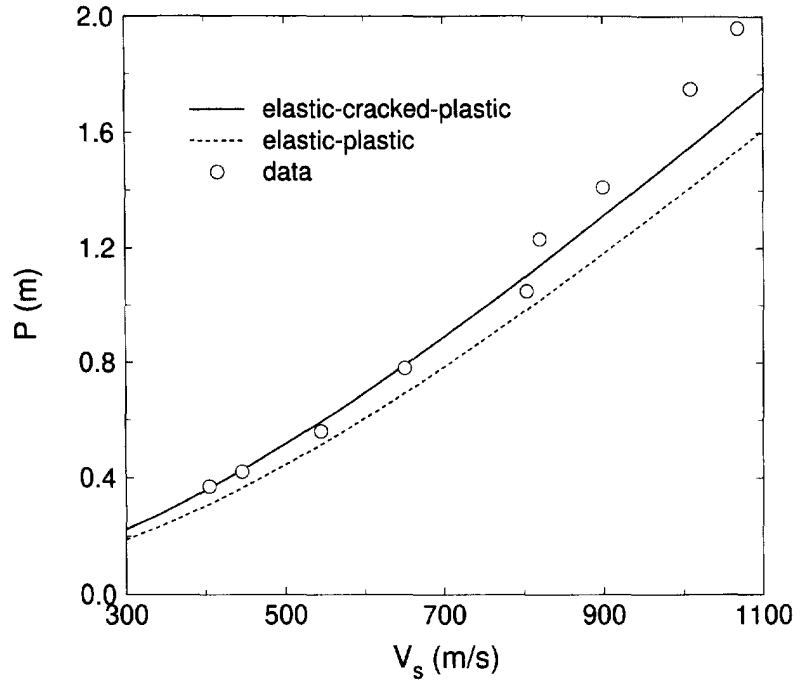

Fig. 10. Depth of penetration data and compressible model predictions.

material data in Fig. 2 are for pressures less than 600 MPa. Maximum pressure occurs at the ogive-nose tip, and for these material and projectile parameters, a pressure of 600 MPa corresponds to a rigid-body projectile velocity of 530 m/s. For $V_s = 1100$ m/s, our model estimates a peak pressure of 1100 MPa. Thus, our model predictions use material data estimates well beyond the data range.

SUMMARY

We developed a spherical, cavity-expansion penetration model for concrete targets. Predictions from our compressible model for depth of penetration vs striking velocity are in reasonably good agreement for a concrete target for which we have both triaxial material data and depth of penetration data.

Acknowledgements—This work was supported by the Joint DoD/DOE Munitions Technology Development Program.

REFERENCES

Bishop, R. F., Hill, R. and Mott, N. F. (1945) The theory of indentation and hardness. *Proceedings of the Physical Society* **57,** 147–159.

Chou, P. C. and Hopkins, A. K. (1972) *Dynamic Response of Materials to Intense Impulse Loading.* Air Force Materials Laboratory, Wright-Patterson AFB, Ohio, pp. 67–70.

Fleck, N. A., Stronge, W. J. and Liu, J. H. (1990) High strain-rate shear, response of polycarbonate and polymethyl methacrylate. *Proceedings of the Royal Society of London* **A429,** 459–479.

Forrestal, M. J. (1986) Penetration into dry porous rock. *International Journal of Solids and Structures* **22,** 1485–1500.

Forrestal, M. J. and Luk, V. K. (1988) Dynamic spherical cavity-expansion in a compressible elastic–plastic solid. *Journal of Applied Mechanics* **55,** 275–279.

Forrestal, M. J. and Longcope, D. B. (1990) Target strength of ceramic materials for high-velocity penetration. *Journal of Applied Physics* **67,** 3669–3672.

Forrestal, M. J., Luk, V. K., Rosenberg, Z. and Brar, N. S. (1992) Penetration of 7075-T651 aluminum targets with ogival-nose rods. *International Journal of Solids and Structures* **29,** 1729–1736.

Forrestal, M. J. and Luk, V. K. (1992) Penetration into soil targets. *International Journal of Impact Engineering* **12,** 427–444.

Forrestal, M. J., Hanchak, S. J., Young, E. R. and Ehrgott, J. W. (1992) Perforations of concrete slabs with 48 MPa (7 ksi) and 140 MPa (20 ksi) unconfined compressive strength. *International Journal of Impact Engineering* **12,** 1–7.

Forrestal, M. J., Altman, B. S., Cargile, J. D. and Hanchak, S. J. (1994) An empirical equation for penetration depth of ogive-nose projectiles into concrete targets. *International Journal of Impact Engineering* **15,** 395 405.

Forrestal, M. J., Tzou, D. Y., Askari, E. and Longcope, B. D. (1995) Penetration into ductile metal targets with rigid spherical-nose rods. *International Journal of Impact Engineering* **16,** 699–710.

Forrestal, M. J., Frew, D. J., Hanchak, S. J. and Brar, N. S. (1996) Penetration of grout and concrete targets with ogive-nose steel projectiles. *International Journal of Impact Engineering* **18,** 465–476.

Goodier, J. N. (1965) On the mechanics of indentation and cratering in the solid targets of strain-hardening metal by impact of hard and soft spheres. *Proceedings of the 7th Symposium on Hypervelocity Impact III*, 215–259.

Hill, R. (1948) A theory of earth movement near a deep underground explosion. Memo No. 21-48, Armament Research Establishment, Fort Halstead, Kent, U.K.

Hill, R. (1950) *The Mathematical Theory of Plasticity*. Oxford University Press, London.

Hopkins, H. G. (1960) Dynamic expansion of spherical cavities in metals. In *Progress in Solid Mechanics*, Vol. 1, Chapter III, eds. I. N. Sneddon, and R. Hill. North-Holland Publishing Company, Amsterdam, New York.

Joy, S. and Ehrgott, J. Q. (1993) Material Characterization of SAC-5 Concrete. Private communication, U.S. Army Waterways Experiment Station, Vicksburg, MS 39180-6199.

Mellegard, K. D., Pfeifle, T. W., Fossum, A. L. and Senseny, P. E. (1993) Pressure and flexible membrane effects on direct-contact extensometer measurements in axisymmetric compression tests. *Journal of Testing and Evaluation* **21,** 530–538.

Press, W. H., Flannery, B. P., Teukolsky, S. A. and Vetterling, W. T. (1989) *Numerical Recipes, The Art of Scientific Computing*. Cambridge University Press, New York.

Radin, J. and Goldsmith, W. (1988) Normal projectile penetration and perforation of layered targets. *International Journal of Impact Engineering* **7,** 229–259.

Satapathy, S. and Bless, S. (1995) Cavity expansion analysis of brittle materials. In *Proceedings of the* 1995 *International Conference on Metallurgical and Materials Applications of Shock-Wave and High-Strain-Rate Phenomena*, eds L. E. Murr, K. P. Staudhammer and M. A. Myers. Elsevier Science Ltd., Oxford, pp. 187–194.

Wright, S. C., Huang, Y. and Fleck, N. A. (1992) Deep penetration of polycarbonate by a cylindrical indenter. *Mechanics of Materials* **13,** 227–284.

Wright, S. C., Fleck, N. A. and Stronge, W. J. (1993) Ballistic impact of polycarbonate—an experimental investigation. *International Journal of Impact Engineering* **13,** 1–20.